

## THE SYSTEM Fe–Co–Ni–As–S. I. PHASE RELATIONS IN THE (Fe,Co,Ni)As<sub>0.5</sub>S<sub>1.5</sub> SECTION AT 650° AND 500°C

SKAGE R. HEM<sup>§</sup> AND EMIL MAKOVICKY

*Geological Institute, University of Copenhagen, Østervoldgade 10, DK-1350 København K, Denmark*

### ABSTRACT

The phase relations in the sulfur-rich regions of the system Fe–Co–Ni–As–S were investigated with mineral syntheses, and characterization of the products by electron-microprobe analysis and powder X-ray diffraction. The experimental charges were weighed with an atomic ratio (Fe + Co + Ni)/(As + S) of 1:2 and a S:As ratio of 3:1. Two isothermal sections were investigated, 500° and 650°C. The 500°C experiments resulted in the formation of arsenopyrite, cobaltite, cattierite, gersdorffite, linnaeite, monosulfide solid-solution, pyrite, siegenite and vaesite. Pyrite, the most common phase, is found in all Fe-bearing assemblages. The phase assemblages formed at 650°C involve cattierite, vaesite, cobaltite and gersdorffite in Fe-poor samples. In Fe-rich samples, the phase assemblage is dominated by monosulfide solid-solution and As<sub>1-x</sub>S<sub>x</sub> melt. The formation of this melt made it possible to estimate the activity of sulfur, using the constraints of Barton (1969). Cobaltite, cattierite and gersdorffite all show extensive solid-solution with respect to Co–Ni and As–S. All the *Me*(As,S)<sub>2</sub> phases have a pyrite-type structure with a disordered distribution of As and S (space group *Pa3*); the unit-cell parameter *a* was determined.

*Keywords:* cattierite, cobaltite, gersdorffite, vaesite, monosulfide solid-solution, *mss*, As–S melt, unit-cell size, linnaeite, siegenite, phase relations.

### SOMMAIRE

Nous avons établi les relations de phases dans les régions riches en soufre du système Fe–Co–Ni–As–S par synthèse de minéraux, et par caractérisation des produits par analyses avec une microsonde électronique et par diffraction X (méthode des poudres). Les réactifs ont été préparés avec un rapport atomique (Fe + Co + Ni)/(As + S) de 1:2 et un rapport S:As de 3:1. Nous avons choisi deux sections isothermales, 500° et 650°C. Les expériences à 500°C ont donné les phases arsenopyrite, cobaltite, cattierite, gersdorffite, linnaeite, solution solide monosulfurée, pyrite, siegenite et vaesite. La pyrite, la phase la plus répandue dans les produits, est présente dans tous les assemblages contenant du fer. Les assemblages formés à 650°C contiennent cattierite, vaesite, cobaltite et gersdorffite dans les échantillons à faible teneur en Fe. Dans les échantillons riches en Fe, les assemblages contiennent en prépondérance la solution solide monosulfurée et un bain fondu As<sub>1-x</sub>S<sub>x</sub>. La formation de ce liquide nous a permis d'estimer l'activité du soufre, en utilisant les contraintes de Barton (1969). La cobaltite, la cattierite et la gersdorffite montrent toutes une solution solide étendue par rapport à Co–Ni et As–S. Toutes les phases *Me*(As,S)<sub>2</sub> ont une structure de type pyrite, avec une distribution désordonnée de As et S (groupe spatial *Pa3*); nous en avons déterminé le paramètre réticulaire *a*.

(Traduit par la Rédaction)

*Mots-clés:* cattierite, cobaltite, gersdorffite, vaesite, solution solide monosulfurée, *mss*, bain fondu As–S, dimensions de la maille, linnaeite, siegenite, relations de phases.

### INTRODUCTION

The Fe–Co–Ni–As–S system contains several important sulfides, sulfarsenides and diarsenides common in complex Co–Ni–As deposits such as Bou-Azzer, Morocco (En Nacri 1995), the Cobalt District, Ontario (Petruk *et al.* 1971), Modum, Norway (Grorud 1997) and Spessart, Germany (Wagner & Lorenz 2002). The As-rich part of the Fe–Co–Ni–As–S system, the (Fe, Co,

Ni)As<sub>1.5</sub>S<sub>0.5</sub> section, is treated in a companion paper (Hem & Makovicky 2004). In this paper, we treat the sulfur-rich part of the system, the (Fe,Co,Ni)As<sub>0.5</sub>S<sub>1.5</sub> section, describe the phase relations involving sulfarsenides, disulfides, monosulfide solid-solution, siegenite, linnaeite and As<sub>1-x</sub>S<sub>x</sub> melt. In preparing the two papers as a joint contribution, we aim to describe the phase relations involving the solid solutions of the sulfarsenides of Fe, Co and Ni.

<sup>§</sup> E-mail address: skage@geol.ku.dk

## BACKGROUND INFORMATION

Several subsystems of the system Fe–Co–Ni–As–S have been investigated at temperatures comparable to those explored in this study. In relation to this work, the most important ones are the system: Fe–As–S (Barton 1969), Fe–Co–Ni–As–S and Fe–Co–Ni–S<sub>2</sub> (Klemm 1965), Ni–As–S (Yund 1962), Co–Fe–S (Wyzomirski 1980), Ni–Fe–S (Kullerud *et al.* 1969, Craig & Scott

1974) and Co–Ni–S (Lamprecht 1978), each describing a limited portion of the relevant compositional space. Those of the contributions that are applicable to the (Fe,Co,Ni)(As,S)<sub>2</sub> prism are schematically summarized in Figure 1. The phase equilibria reported involve coexistence of corresponding disulfides and sulfarsenides, and disulfides and thiospinels or monosulfide solid-solution (*mss*). Complete solid-solutions are reported between CoS<sub>2</sub> and NiS<sub>2</sub>, and among FeS<sub>1-x</sub>, CoS<sub>1-x</sub> and

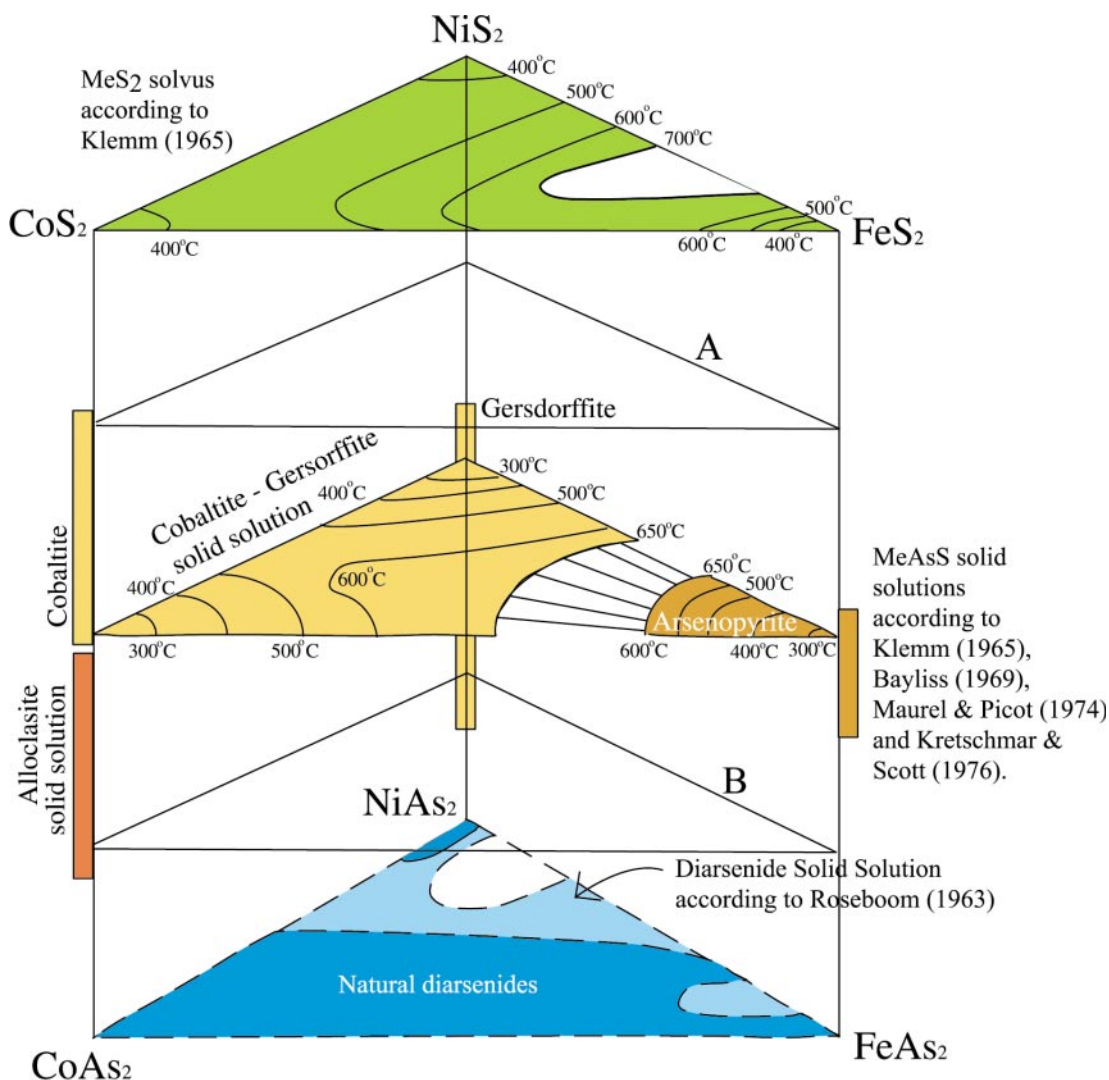


FIG. 1. Schematic presentation of the (Fe,Co,Ni)(As,S)<sub>2</sub> prism illustrating previous studies of the Fe–Co–Ni–As–S system. The plane *A* shows the bulk composition of the charges used in this study, whereas *B* shows the bulk compositions of the charges used in the companion paper (Hem & Makovicky 2004). The reported variation in As–S content of each phase is shown by bars at the relevant y-axis. The variations in Fe–Co–Ni contents are drawn as fields at the appropriate As–S content. Compositional isotherms are sketched where available. Additional references are quoted in the text.

$\text{Ni}_{1-x}\text{S}$ . Solid solution is extensive between Fe end-members and  $(\text{Ni}, \text{Co})\text{S}_2$  and  $(\text{Ni}, \text{Co})\text{AsS}$ , as well as that involving Ni in  $\text{Co}_3\text{S}_4$  and monosulfide solid-solution (*mss*).

There are few natural analogues to the investigated system, and these are poorly constrained with respect to temperature. Cattierite and vaesite usually form at low temperatures by the replacement or remobilization of previously deposited Co- and Ni-bearing minerals, although primary vaesite has been found in Kuroko-type ores (Sato & Shimazaki 1975). The formation of cattierite or vaesite is generally associated with talc-carbonate alteration of mafic rocks (Hudson & Groves 1974, Ostwald 1980, Burke & Zakrzewski 1983, Barnes & Hill 2000), in which the disulfides usually replace or overgrow an older assemblage of sulfides. Abbreviated mineral names used in the text are given in Table 1.

#### EXPERIMENTAL PROCEDURES

Experimental charges totaling 200 mg were weighed using pure elements supplied by Alpha Aesar: Fe (Puratronic, 99.995%), Co (Puratronic, 99.995%), Ni

(99.997% Ni), As (Puratronic, 99.9999%) and S (Puratronic, 99.9995%). The metals were supplied as solid rods, which were filed using a steel file. Each file was used for separate elements. The first batch of shavings was discarded. This was done to minimize contamination from possible products of oxidation and from the file. Trace amounts of Fe were found in supposedly Fe-free samples, and it is believed that this Fe originated from the sample preparation. Sulfur was supplied in the form of tiny flakes, which could be easily crushed into the desired size and added to the sample using a pair of tweezers. Arsenic was supplied as lumps with a diameter of 0.5–1 cm. These were hand crushed in an agate mortar. Arsenic was prepared shortly before sample evacuation (<4 hrs), and no visible oxidation was evident. Unused arsenic was stored in evacuated glass tubes.

The charge compositions corresponded the stoichiometry  $(\text{Fe}, \text{Co}, \text{Ni})\text{As}_{0.5}\text{S}_{1.5}$ . In the 650°C experiments, 66 charges with different Fe, Co and Ni contents were weighed out, at intervals of 3.33 at.% (Fig. 2). The 25 charges examined in the 500°C experiments were placed along the binary joins as well as lines corresponding to

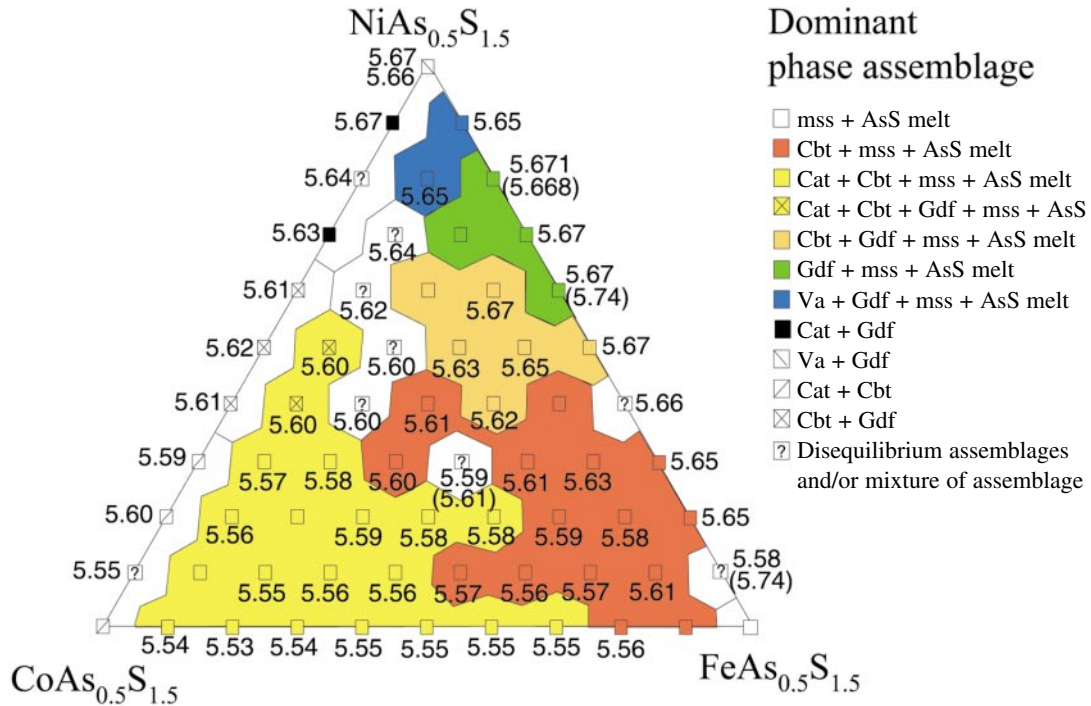


FIG. 2. Phase assemblage formed at 650°C, plotted according to the composition of the experimental charges. The triangle shown corresponds to bulk compositions located in the  $(\text{Fe}, \text{Co}, \text{Ni})\text{As}_{0.5}\text{S}_{1.5}$  plane (A in Fig. 1). The legend lists the dominant phase-assemblage in each sample. The refined unit-cell parameter  $a$  of the dominant  $\text{MeX}_2$  phase is written alongside each charge composition. In some case, two unit cells could be discerned, in which case both are listed. The data are rounded off; full data are available in Appendix C (deposited).

( $\text{Fe}_{0.80-x}\text{Co}_x\text{Ni}_{0.20}$ ) $\text{As}_{0.5}\text{S}_{1.5}$ , ( $\text{Fe}_{0.65-x}\text{Co}_x\text{Ni}_{0.35}$ ) $\text{As}_{0.5}\text{S}_{1.5}$  and ( $\text{Fe}_{0.5}\text{Co}_x\text{Ni}_{0.5-x}$ ) $\text{As}_{0.5}\text{S}_{1.5}$ , and a few charges of ternary composition close to each of the metal corners. The sample material was filled into silica tubes, which were sealed under vacuum (0.001–0.005 atm). The charges were heated for three or four periods of three months; between these annealing intervals, they were reground. The typical grain-size of the products was 10–100  $\mu\text{m}$ . Temperatures were measured using two independent chromel–alumel thermocouples. One thermocouple was attached to the charges, and the other was connected to a Eurotherm 91e PID control unit thermostatically regulating the temperature ( $\pm 0.25^\circ\text{C}$ ). The temperature variation within the experimental area of the furnace was found to be  $\pm 2.8^\circ\text{C}$ . The average thermal degradation of the thermocouples was found to be up to  $+2.4^\circ\text{C}$ , indicating that the temperature increased slightly during the experiments. At the end of the experiment, the charges were quenched in cold water. In order to facilitate equilibration, a LiCl–KCl melt was added one week before the termination of the experiment. At this point, the samples also were reground. The halide melt was washed out of the samples before sample preparation.

#### ANALYTICAL METHODS

The sample material was split in two. One part was prepared as polished sections, and the other was investigated by powder X-ray diffraction. The polished sections were investigated by means of optical microscopy and analyzed with an electron microprobe.

#### Powder X-ray diffraction (PXRD)

Pulverized samples were investigated on a Philips PW 3710 diffractometer using  $\text{CuK}\alpha$  radiation. The samples were investigated in the  $2\theta$  range from  $10^\circ$  to  $80^\circ$ , with a step size of  $0.020^\circ$  and counting time of 10 seconds. Data were treated using the Bruker EVA program; we subtracted the background and  $K\alpha_2$  radiation. In samples rich in  $\text{As}_{1-x}\text{S}_x$  glass (see below), a significant positive bulge in the background could be seen over the  $2\theta$  interval  $15^\circ$ – $40^\circ$ .

Except for minor variations, the diffraction data suggest the presence of several isostructural  $\text{Me}(\text{S},\text{As})_2$  phases ( $\text{Me}$  represents the sum of metals) with a pyrite structure, as well as monosulfide solid-solution (*mss*). All the cubic  $\text{Me}(\text{S},\text{As})_2$  phases found in this study crystallize in space group  $Pa\bar{3}$ , and show no signs of As–S order. The distinction between such cubic  $\text{Me}(\text{S},\text{As})_2$  phases is hampered by the structural and chemical similarity of the phases. It is especially difficult to discern gersdorffite ( $5.688 < a < 5.705 \text{ \AA}$ ; Bayliss 1968, Bayliss & Stephenson 1968) from vaesite ( $5.676 < a < 5.687 \text{ \AA}$ ; Elliot 1960, Furuseh & Kjekshus 1969, Nowack *et al.* 1989); cobaltite ( $5.576 < a < 5.583 \text{ \AA}$ ; Giese & Kerr 1965, Steger *et al.* 1974, Fleet & Burns 1990) and cattierite ( $5.523 < a < 5.539 \text{ \AA}$ ; Elliot 1960, Pratt &

Bayliss 1979) also are difficult to discern owing to the extensive substitution between As and S. Disulfides and sulfarsenides can be discerned on the basis of the intensity ratios between different reflections. The ratio between the calculated intensities of the (111) and the (210) reflections is higher than 20:1 in disulfides, whereas it is 1:10 for sulfarsenides. The majority of samples from this study have low ratios ( $\sim 1:5$ ), indicating that the samples are dominated by sulfarsenides. There are a number of systematically occurring peaks in the  $2\theta$  intervals  $29$ – $30^\circ$  and  $33$ – $34^\circ$ . Their intensity correlates with the intensity of the *mss* peaks, and it is possible that these reflections are produced by *mss* superstructures.

In most samples from the  $650^\circ\text{C}$  experiments, only a single  $\text{Me}(\text{S},\text{As})_2$  phase could be identified on the basis of its PXRD pattern. Electron-microprobe analysis revealed that several  $\text{Me}(\text{S},\text{As})_2$  phases are present. We thus believe that the observed PXRD pattern is the result of overlap among closely related patterns. In order to address this problem, we calculated the unit-cell parameters of the  $\text{Me}(\text{S},\text{As})_2$  phases, and examined their dependence on charge composition with a multiple regression [ $a \text{ (\AA)} = 5.684 \text{ (\AA)} - 0.065 \text{ Fe (at.\%)} - 0.170 \text{ Co (at.\%)}; R = 0.855, n = 63$ ]. Within the uncertainty of the regression,  $a$  follows the same general tendency as the data of Klemm (1965) for the cobaltite–gersdorffite solid-solution series. The residuals of the regression revealed that at least two groups of samples are present. By comparing with the EMPA data, it became apparent that these groups correspond to samples dominated by gersdorffite, cattierite or cobaltite. The unit-cell parameter  $a$  depends on charge composition (Fig. 2; data are listed in Appendix C, deposited). Selected joins showing the variation of unit-cell parameter  $a$  with charge compositions are presented in Figure 3; these correspond to the sides of the compositional triangle, as well as the  $\text{Fe}_{0.3}\text{Co}_{0.7} - \text{Ni}_{0.3}\text{Co}_{0.7}$  section. The dominant phase or phases are written at the lines, and the abrupt changes in the evolution of these lines document changes in phase assemblage. The line defined by the cattierite- and cobaltite-bearing charges (Cat + Cbt) and cattierite- and gersdorffite-bearing charges (Cat + Gdf) corresponds well with the relation found by Hanus & Mushi (1971) for the cattierite–vaesite solid solution, except that their cattierite is  $0.02 \text{ \AA}$  smaller. The disulfides thus are dominant phases in these assemblages.

The unit-cell parameters from the phases formed during the  $500^\circ\text{C}$  experiments were calculated for most of the phases. They are listed for the relevant compositions in Appendix B (deposited). These unit-cell parameters are shown in Figure 4, where they are plotted against at.% S and the average effective ionic radius ( $IR$ , Shannon 1976) of the metals. The latter was calculated by assuming that all metals are divalent and in a low-spin configuration, and then multiplying the corresponding value of  $IR$  by the relative concentration of the metals. Cobaltite, gersdorffite and cattierite all show a

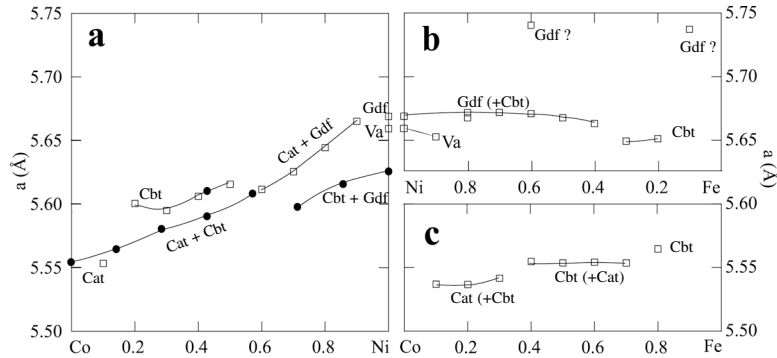


FIG. 3. The empirical unit-cell parameter  $a$  of  $Me(As,S)_2$  phases versus charge composition. All data are from the 650°C experiments and shown as sections along selected lines in the  $(Fe,Co,Ni)As_{0.5}S_{1.5}$  triangle. Squares denote data from the sides of the triangle, (a) Co – Ni, (b) Ni – Fe and (c) Co – Fe join. The filled circles in (a) are data along the  $(Co,Ni)_{0.7}Fe_{0.3}$  line. The dominant phase or phases contributing to the diffraction data are written at the data points; phases in parentheses are believed to have had little influence on the unit cell, those with question marks denote cases of disequilibrium, which also have very large standard deviations.

positive correlation between  $IR$  and unit-cell parameter  $a$  (Fig. 4b). Pyrite and vaesite show a weak correlation or none at all. The gersdorffite samples that lie on the marked line are all from vaesite-free assemblages, suggesting that peak overlap between gersdorffite and vaesite has had an effect, causing the calculated unit-cell of the gersdorffite not to lie on the line. All  $Me(S,As)_2$  phases seemingly show a weak positive correlation between sulfur content and unit-cell parameter  $a$ . This is most likely an artificial correlation caused by the covariance of  $IR$  and  $S\%$ , as substitution of As by S is expected to decrease the unit-cell size, and thus the unit-cell parameter  $a$ .

Other phases detected include sulfate hydrates of Co and Ni, as well as kaatialaite ( $FeAs_3O_9 \cdot 8.25 H_2O$ ) and arsenolite ( $As_2O_3$ ). These phases formed after the experiments, by reactions between the experimental products and the water used to wash out the halide flux or hygroscopic water attracted by possible Li-flux remnants. The hydrated phases were not observed in the

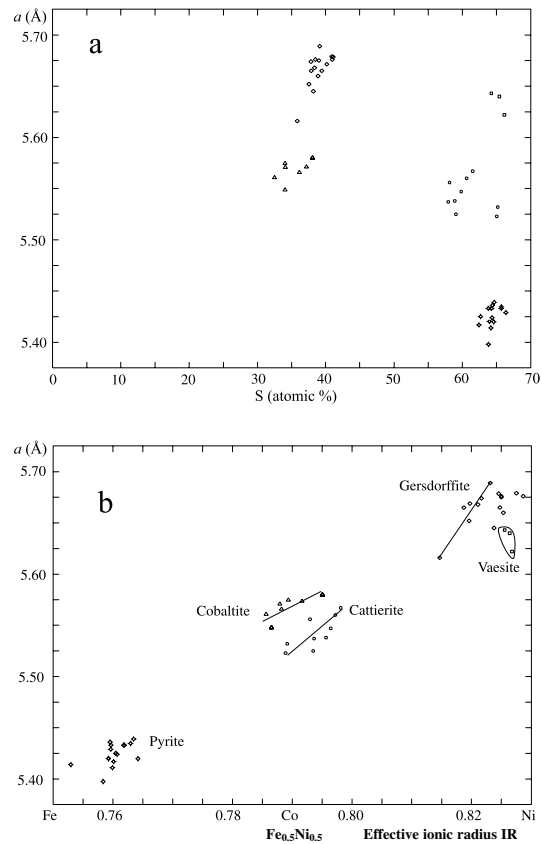


FIG. 4. Variation in unit-cell parameter  $a$  plotted with (a) at.% S and (b) the average effective ionic radius of the metals,  $IR$ , from the 500°C experiments. The weak positive correlations with S contents in cobaltite and gersdorffite are most likely produced by the covariance between Ni and S. In cobaltite and cattierite, there are clear positive correlations between  $IR$  and  $a$ . For gersdorffite, this relation is apparent only in vaesite-free assemblages.

polished sections or during EMPA, probably because the polished sections were prepared immediately after the experiments, whereas there was a waiting period of up to 8 months before the PXRD analyses were performed.

#### Electron-microprobe analysis (EMPA)

Wavelength-dispersion electron-microprobe analyses were performed on a JEOL JcXA-733 Superprobe, using a focused beam. Accelerating voltage was set to 20 kV, and the beam current was 20 nA. The samples were analyzed using FeK $\alpha$ , CoK $\alpha$ , NiK $\alpha$ , SK $\alpha$  and AsL $\alpha$ . Arsenopyrite (Asp200 of Kretschmar & Scott 1976) and pyrite, as well as pure Co and Ni metal, were used as primary standards. Results of the analyses are tabulated in Appendices A, B and C. These are available from the Depository of Unpublished Data, CISTI, National Research Council, Ottawa, Ontario K1A 0S2, Canada.

#### EXPERIMENTAL RESULTS

The reported equilibria were established by optical microscopy and by analyzing intergrown phases with EMPA. The mineral names ascribed to the different phases are given in accordance to the corresponding natural phase by combining the optical and chemical observations with PXRD data. This correspondence is uncertain for gersdorffite and cobaltite found at 650°C, as the observed compositions are much richer in sulfur than the natural analogues. The phase assemblages observed are listed in Table 1.

Phase assemblages, textures and compositions all indicate that overall equilibrium was seldom reached. Only a few samples achieved equilibrium, characterized by granular textures with triple junctions, homogeneous

compositions and grain sizes, as well as a uniform assemblage throughout the charge. Observations from such samples defined a framework for the interpretation of the less clear cases.

Most samples show minor evidence of disequilibrium. They are dominated by a single phase-assemblage, but the composition of the phases varies somewhat. Typical chemical traits of these samples are: minor changes in solid-solution limits dependent on charge composition, trend-like compositional variation of co-existing phases, and compositional differences between analogous phase-assemblages from the same sample. The grain size of these phases varies, they contain few inclusions, and they may exhibit textures indicating replacement.

Another group of samples shows large degrees of disequilibrium; several phase-assemblages are present in the same sample, seemingly unrelated compositions are found within an aggregate as are zoned aggregates and corona textures, and there is an arbitrary orientation of tielines. Samples showing a large degree of disequilibrium were not directly used when determining phase relations, although observations from such samples were useful when interpreting related samples.

In the 500°C experiments, the phase assemblages are generally richer in metals than the  $MeS_{1.5}As_{0.5}$  bulk composition. This enrichment most likely is due to loss of sulfur during sample regrinding. This loss moved the charge composition from the  $MeAsS - MeS_2$  line into the  $MeAsS - MeS_2 - mss$  triangle. In samples poor in Fe, linnæite or siegenite thus formed instead of *mss*. A similar loss of sulfur probably also occurred in the 650°C experiments, but the loss of sulfur was not large enough to displace the sample from the  $Me(S,As)_2 - mss - AsS$  triangle, which constitutes the principal phase-assemblage at 650°C.

TABLE 1. PHASE ASSEMBLAGES IN THE SYSTEM Fe-Co-Ni-As-S AT 650° AND 500°C

T(°C)	Five phases	Four phases	Three phases	Two phases
650	Cbt + Gdf + Cat + <i>mss</i> + AsS	Cbt + Cat + <i>mss</i> + AsS Cbt + Gdf + <i>mss</i> + AsS Gdf + Va + <i>mss</i> + AsS	Cbt + <i>mss</i> + AsS Gdf + <i>mss</i> + AsS	Cbt + Cat Gdf + Cat Gdf + Va
500	Apy + Cbt + Gdf + Py + <i>mss</i> Cbt + Gdf + Py + Cat ± <i>mss</i> Gdf + Py + Cat + Va ± <i>mss</i>	Apy + Gdf + Py + <i>mss</i> Apy + Cbt + Py + <i>mss</i> Cbt + Gdf + Py + <i>mss</i> Cbt + Gdf + Cat + Lin Cbt + Py + Cat + <i>mss</i> Cbt + Cat + <i>mss</i> + Lin Gdf + Py + Va + <i>mss</i> Gdf + Cat + Va + Sie	Apy + Py + <i>mss</i> Gdf + Cat + Lin Gdf + Py + <i>mss</i>	Cbt + Py

The mineral abbreviations used in this table and throughout the text are: Apy: arsenopyrite, AsS:  $As_{1-x}S_x$  melt, Cat: catterite, Cbt: cobaltite, Gdf: gersdorffite, Lin: linnæite, *mss*: monosulfide solid-solution, Py: pyrite, Sie: siegenite, Va: vaesite.

## THE 650°C EXPERIMENTS

The phase relations in the compositional space straddling the (Fe,Co,Ni)As<sub>0.5</sub>S<sub>1.5</sub> triangle can be described as combinations of the phase associations found at each of the metal corners. In the Fe corner, the equilibrium assemblage is monosulfide solid-solution (*mss*) and As<sub>1-x</sub>S<sub>x</sub> melt (AsS), in the Co corner, it is cobaltite (Cbt) and cattierite (Cat), and in the Ni corner, it is gersdorffite (Gdf) and vaesite (Va).

Cattierite, cobaltite, gersdorffite and *mss* display extensive solid-solutions, and the dominant phase-associations are Cat + Cbt + *mss* + AsS, Cbt + Gdf + *mss* + AsS and Cbt + *mss* + AsS. These meet in the five-phase assemblage Cat + Cbt + Gdf + *mss* + AsS. The phase compositions from the five-phase assemblages are given in Table 2. Figure 2 shows the distribution of the observed phase-equilibria compared to the bulk composition of the samples. Rare disequilibrium-induced products, *i.e.*, siegenite, violarite, pyrite and arsenopyrite, were also encountered.

As<sub>1-x</sub>S<sub>x</sub> melt

The sulfur-arsenic glass encountered in the experiments is interpreted as quenched As<sub>1-x</sub>S<sub>x</sub> melt, which was stable at higher temperature. Previous studies of related systems (Clark 1960) have shown that the glass maintains its composition when quenched. This state-

ment is corroborated by the systematic relation between the composition of the glass and the compositions of the coexisting solid phases (Fig. 5).

The composition of the As<sub>1-x</sub>S<sub>x</sub> melt (42.9–60.8 at.% S, 39.1–56.7 at.% As and 0.00–0.67 at.% Me) varies greatly according to paragenesis (Fig. 5), but there is also significant compositional variation within each phase-assemblage, especially the Cbt + *mss* + AsS melt assemblage. The metal content varies independently of As-S contents and paragenesis, and is therefore believed to be the result of interference from neighboring grains, or inclusions in the melt, during EMPA. The composition of the melt can therefore be written As<sub>1-x</sub>S<sub>x</sub>, where 0.43 < x < 0.61.

The compositions of the melt agrees with the compositional ranges for As<sub>1-x</sub>S<sub>x</sub> melt coexisting with pyrrhotite as found by Barton (1969), and according to his diagrams, the compositional range 39.1–56.7 at.% As corresponds to log *a*(S<sub>2</sub>) values of approximately –3.0 to –1.1 (listed in Appendix C, deposited). The log *a*(S<sub>2</sub>) values are written next to the tielines of each phase assemblage in the relevant figures.

Cattierite, CoS<sub>2</sub>

Cattierite occurs in phase assemblages containing combinations of As<sub>1-x</sub>S<sub>x</sub> melt, cobaltite, gersdorffite, *mss* or linnaeite (Table 1). In addition to Co and S, it can contain up to 3.4 at.% Fe, 24.7 at.% Ni and 9.6 at.%

TABLE 2. PHASE COMPOSITIONS IN THE FIVE-PHASE ASSEMBLAGES IN THE SYSTEM Fe-Co-Ni-As-S AT 650° AND 500°C

T(°C)	Assemblage	Phase	<i>n</i>	at.% S	at.% As	at.% Fe	at.% Co	at.% Ni	Total wt%
650	Cbt + Gdf	Cbt	8	44.7 (0.6)	22.1 (0.6)	4.8 (1.0)	13.9 (1.6)	14.4 (0.7)	101.4 (0.6)
		+ Cat	Gdf	12	44.0 (0.9)	22.8 (0.9)	3.0 (0.6)	8.7 (1.3)	21.5 (1.4)
	+ <i>mss</i>	Cat	9	58.1 (0.9)	8.7 (0.9)	1.1 (0.6)	18.0 (0.9)	14.1 (1.2)	101.8 (0.5)
		+ AsS	<i>mss</i>	7	53.5 (0.3)	0.1 (0.1)	21.6 (0.3)	2.2 (0.1)	22.6 (0.2)
			AsS	3	56.2 (0.1)	43.8 (0.1)	0.0 (0.0)	0.0 (0.0)	0.0 (0.0)
500	Apy + Cbt	Apy	5	34.0 (0.9)	33.6 (0.9)	26.5 (1.1)	5.7 (0.9)	1.3 (0.2)	99.8 (1.1)
		+ Gdf	Cbt	8	35.3 (1.1)	31.1 (1.3)	4.0 (1.2)	23.2 (1.3)	6.5 (1.2)
	+ Py	Gdf	6	36.4 (1.3)	30.1 (1.3)	3.9 (0.5)	2.2 (0.8)	27.5 (1.1)	100.0 (0.9)
		+ <i>mss</i>	Py	6	64.1 (0.9)	2.6 (0.9)	27.4 (0.3)	2.8 (0.3)	3.2 (0.2)
			<i>mss</i>	4	53.8 (0.3)	0.1 (0.1)	44.1 (0.4)	0.5 (0.0)	1.6 (0.1)
500	Cbt + Gdf	Cbt	4	38.0 (0.6)	28.1 (0.6)	2.2 (0.3)	25.2 (0.2)	6.5 (0.3)	101.0 (0.8)
		+ Py	Gdf	6	37.8 (0.5)	29.2 (0.3)	1.3 (0.5)	4.3 (1.1)	27.4 (1.1)
	+ Cat	Py	3	64.4 (0.8)	1.8 (0.8)	27.5 (0.3)	4.5 (0.2)	1.8 (0.1)	99.9 (0.7)
		+ <i>mss</i>	Cat	5	58.6 (1.2)	7.8 (1.4)	1.4 (0.7)	28.6 (1.0)	3.7 (0.5)
			<i>mss</i>	4	54.0 (0.2)	0.1 (0.0)	43.9 (0.5)	0.5 (0.2)	1.6 (0.5)
500	Gdf + Py	Gdf	9	38.5 (1.3)	27.9 (1.3)	1.6 (0.2)	1.0 (0.1)	31.0 (0.4)	100.6 (0.8)
		+ Cat	Py	11	65.7 (0.6)	0.7 (0.5)	26.8 (0.7)	3.8 (0.7)	3.1 (0.5)
	+ Va	Cat	6	59.1 (1.4)	7.2 (1.5)	2.8 (0.6)	25.3 (1.7)	5.7 (1.3)	100.3 (1.5)
		+ <i>mss</i>	Va	4	65.3 (1.2)	1.0 (1.2)	0.6 (0.1)	2.6 (1.0)	30.4 (1.2)
			<i>mss</i>	6	53.5 (0.4)	0.1 (0.0)	26.9 (1.1)	0.5 (0.2)	19.1 (0.7)

The mineral abbreviations used are the same as in Table 1; *n* represents the number of analyses made. Standard deviation of the average is given in parentheses.

As in solid solution. The cattierite richest in Ni coexists with gersdorffite, and the compositions richest in iron are found in the Cat + Cbt + *mss* + AsS assemblage.

Figure 6 shows compositions of mineral phases from the Cat + Cbt + *mss* + AsS assemblage. The compositions of cattierite, cobaltite and *mss* lie on three subparallel lines, ranging from Ni-free compositions to compositions where approximately half of the metals have been exchanged for Ni. Along this line, cattierite compositions range from (62.8 at.% S, 3.7 at.% As, 3.4 at.% Fe, 30.1 at.% Co) to (58.1 at.% S, 8.7 at.% As, 1.1 at.% Fe, 18.0 at.% Co, 14.1 at.% Ni), and thus show a clear decrease in S content as Ni is introduced.

#### Gersdorffite, NiAsS

Gersdorffite coexists with any of vaesite, cattierite, cobaltite, *mss* or  $As_{1-x}S_x$  melt (Table 1). Its compositions lie in the ranges 43.8–51.6 at.% S, 14.8–22.7 at.% As, 0.0–3.3 at.% Fe, 0.0–19.4 at.% Co and 13.8–33.5 at.% Ni. The gersdorffite richest in Ni and S coexists with vaesite, that richest in Co and S, with cattierite, and that richest in Fe and As, with cobaltite.

The composition of gersdorffite and that of coexisting phases are shown in Figures 7 and 8. Figure 8 shows that the gersdorffite richest in S coexists with vaesite.

The maximum S content in gersdorffite decreases as Ni is replaced by Co or Fe. The continuation of the gersdorffite solid-solution toward compositions richer in As is shown in Figure 7, illustrating the Gdf + Cbt + *mss* + AsS association. The relation in *Me*–As–S space between Gdf and Cbt is shown in the binary diagrams (Fig. 9), illustrating that the volume occupied by the gersdorffite solid-solution is richer in S and Ni than the coexisting cobaltite.

Several cases of textures suggesting breakdown of gersdorffite into S-rich domains (0.2–2.3 at.% Fe, 0.3–2.9 at.% Co, 28.8–32.9 at.% Ni, 48.2–59.7 at.% S and 6.7–18.0 at.% As) and S-poor domains (0.5–2.6 at.% Fe, 0.0–3.9 at.% Co, 26.8–32.1 at.% Ni, 40.0–46.51 at.% S and 20.8–26.8 at.% As) were observed. Both phases have optical characteristics similar to those of gersdorffite, and they could not be distinguished by PXRD. The domains form a vague rectangular pattern, which has replaced part of the host gersdorffite. Compared with the host gersdorffite, the breakdown induced little change in the metal ratios. The compositions richer in S define a trend pointing toward vaesite-like compositions, whereas the products of exsolution poorer in S have compositions corresponding to Fe-poor cobaltite or compositions intermediate between gersdorffite and cobaltite. The true composition of the products is some-

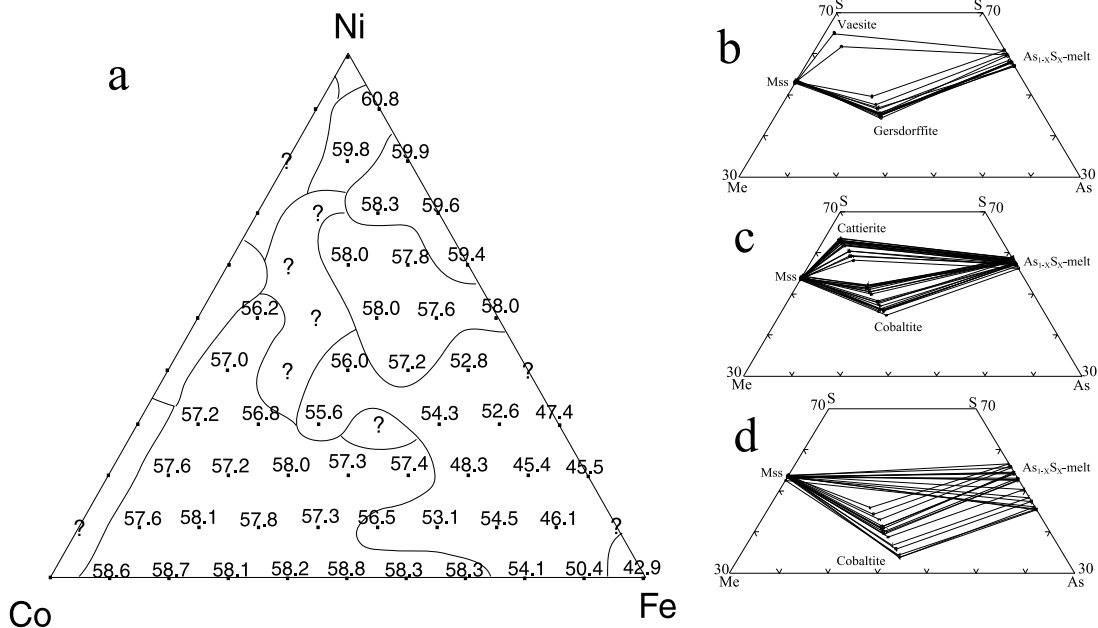


FIG. 5. Composition of the  $As_{1-x}S_x$  melt formed at 650°C. (a) The S content (at.%) of the  $As_{1-x}S_x$  melt shown at the relevant charge compositions. The field is divided according to the mineral assemblages, as shown in Figure 2. (b) *Me*–As–S plots of the Va + Gdf + *mss* + AsS and the Gdf + *mss* + AsS assemblages, (c) the Cat + Cbt + *mss* + AsS assemblage, and (d) the Cbt + *mss* + AsS assemblage.

what uncertain owing to the fine-grained nature of the domains. The two phases are believed to be quench products.

*Cobaltite, CoAsS*

Cobaltite displays a complete solid-solution between Co and Ni and contains 33.7–52.1 at.% S, 14.7–32.7 at.% As and <10.8 at.% Fe. The compositions observed correspond to the S-rich side of the cobaltite solid-solu-

tion, and it most likely continues toward compositions richer in As. The cobaltite richest in Co and S coexists with cattierite (Figs. 6, 9), that richest in Ni and As, with gersdorffite (Fig. 7), and that richest in Fe, with monosulfide solid-solution +  $As_{1-x}S_x$  melt (Fig. 10). The maximum content of sulfur decreases drastically where Co is replaced by Ni. The Co–Fe end member can contain up to 52.1 at.% S (Fig. 6), whereas it can contain approximately 40 at.% S where the Ni content is 0.6 atoms per formula unit (*apfu*) or higher (Fig. 7). Close

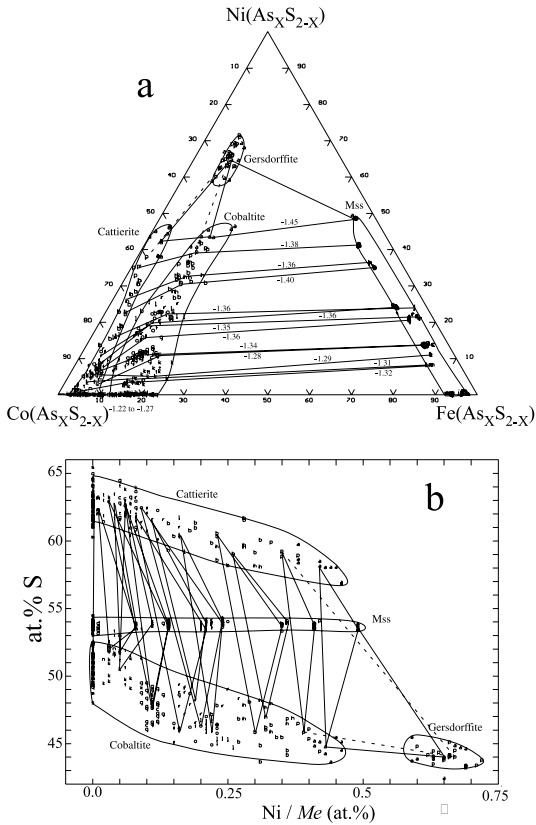


FIG. 6. The compositions of cattierite, cobaltite and *mss* coexisting with  $As_{1-x}S_x$  melt at 650°C, in terms of (a) *apfu* Fe – Co – Ni and (b) at.% S – (at.% Ni / at.% Me). The Ni-rich limit of this assemblage is determined by the appearance of gersdorffite. The tielines are drawn between average compositions of coexisting phases from each charge. The individual analyses on which these averages are based are shown by letters. The composition of the coexisting  $As_{1-x}S_x$  melt extends from approximately  $As_{0.87}S_{1.13}$  for the Ni-free assemblages to  $As_{0.83}S_{1.17}$  for samples richest in Ni. The log  $a(S_2)$  values derived from the  $As_{1-x}S_x$  melt compositions are written at the tielines. The circled fields denote the compositional extremes of each phase for the assemblage. The sulfarsenide formula is given at the corners; the corresponding formula for *mss* is  $(Fe,Co,Ni)_{1-x}S$ .

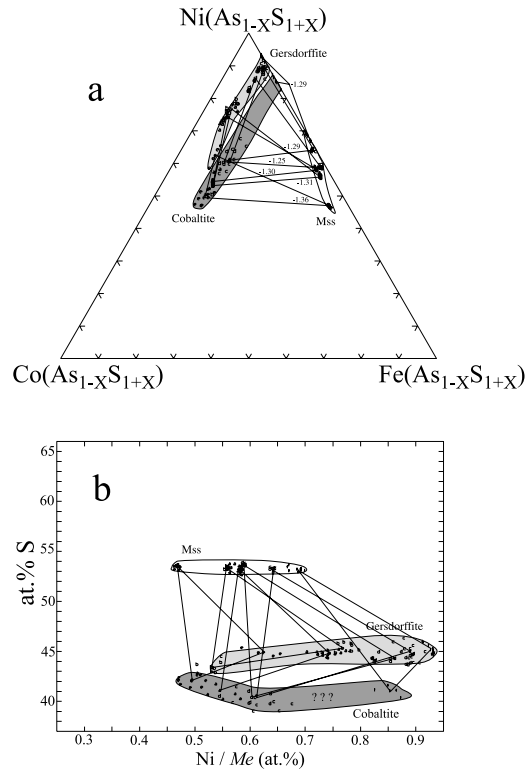


FIG. 7. Cobaltite, gersdorffite and *mss* coexisting with  $As_{1-x}S_x$  melt at 650°C, in terms of (a) *apfu* Fe – Co – Ni and (b) at.% S – at.% Ni / at.% Me. This diagram shows the continuation of the cobaltite solid-solution towards compositions richer in Ni, where it coexists with gersdorffite, *mss* and  $As_{1-x}S_x$  melt. The tielines are drawn between average compositions of coexisting phases from each charge. The individual analytical datasets on which these averages are based are shown by letters. Tielines located on the edges of the diagrams are bent. Gersdorffite is richer in S than the cobaltite it coexists with. The log  $a(S_2)$  values derived from the  $As_{1-x}S_x$  melt compositions are indicated at the tielines. The circled fields denote the compositional extremes of each phase for the assemblage. The sulfarsenide formula is given by the corners, the corresponding formula for *mss* is  $(Fe,Co,Ni)_{1-x}S$ .

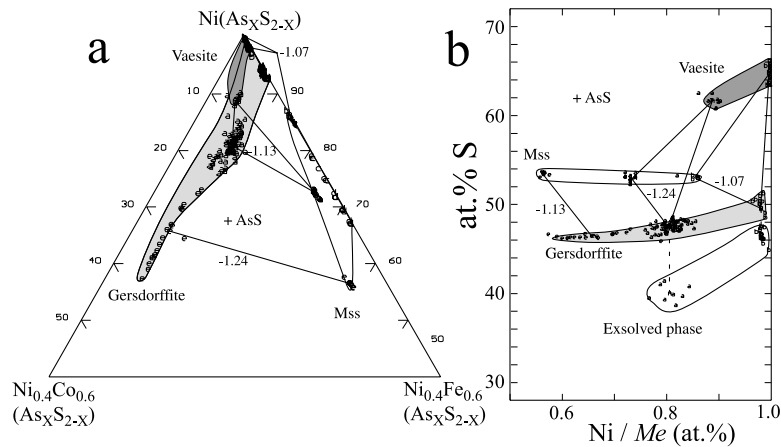


FIG. 8. Compositions of gersdorffite from the Va + Gdf + mss + AsS and the Gdf + mss + AsS assemblages at 650°C, in terms of (a) *apfu* ( $Ni_{0.4}Fe_{0.6}$ ) – ( $Ni_{0.4}Co_{0.6}$ ) – Ni and (b) at.% S – at.% Ni / at.% Me. The tielines are drawn between average compositions of coexisting phases from each charge; the individual analytical datasets on which these averages are based are shown by letters. Tielines are located on the edges of the diagrams are bent. The circled fields denote the compositional extremes of each phase for the assemblage. The continuation of the gersdorffite solid-solution toward compositions richer in As is shown in Figures 2 and 3. The log  $a(S_2)$  values derived from the  $As_{1-x}S_x$  melt compositions are written by the tielines. The “exsolved phase” represents a quench product forming from gersdorffite, together with vaesite. The sulfarsenide formula is given by the corners, the corresponding formula for *mss* is  $(Fe,Co,Ni)_{1-x}S$ .

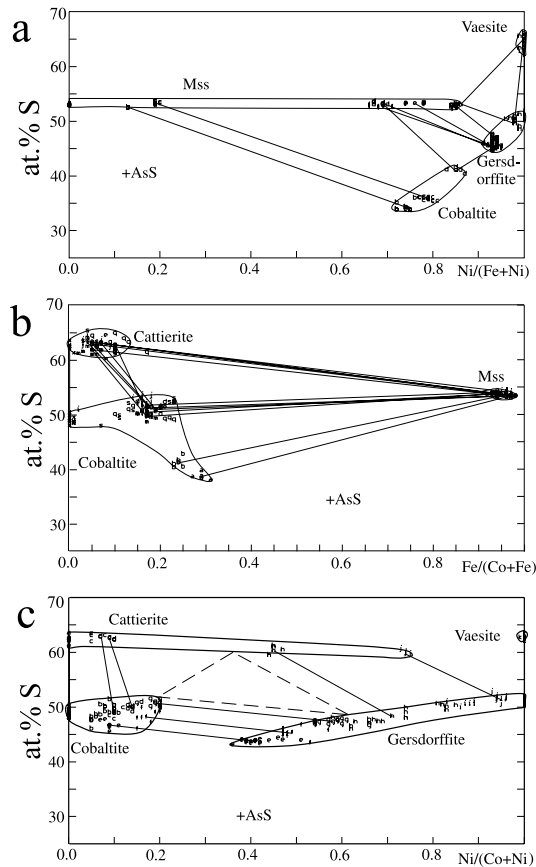


FIG. 9. The Fe–Ni (a), Co–Fe (b) and Co–Ni (c) assemblages formed at 650°C. These figures show the sides of the prism in Figure 14 a and link together Figures 12 and 13. Tielines are drawn between average compositions, based on the analytical datasets indicated by the corresponding letter. The circled fields denote the compositional extremes of each phase in the assemblage in question.

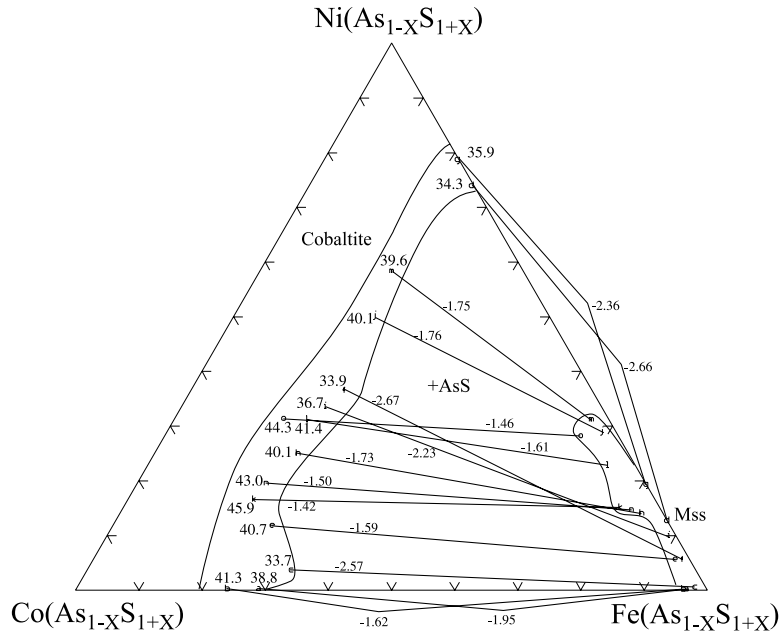


FIG. 10. Average compositions for the Cbt + *mss* + AsS assemblage at 650°C. The tielines between cobaltite and *mss* show a large variation in orientation. This variation is dependent on the  $a(S_2)$ , as Ni is concentrated in cobaltite at low values (Fig. 11). The S content (at.%) of Cbt is written alongside the data points. The sulfarsenide formula is given at the corners; the corresponding formula for *mss* is  $(Fe,Co,Ni)_{1-x}S$ .

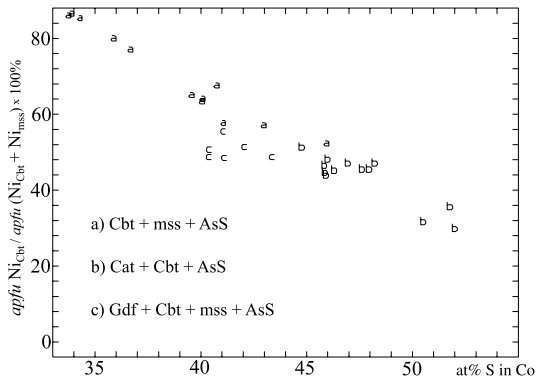


FIG. 11. The proportion of Ni in cobaltite based on the sum of Ni in *mss* and cobaltite, plotted against the S content of cobaltite; *a* marks compositions from the Cbt + *mss* + AsS assemblage, *b*, from the Cat + Cbt + *mss* + AsS assemblage, and *c*, from the Gdf + Cbt + *mss* + AsS assemblage. All data are from the 650°C isotherm.

to the Ni end-member, there is a compositional gap between 0 and 0.2 *apfu* Co (? in Fig. 7). This gap is probably caused by the concentration of Co into cobaltite. The gap could most likely be bridged by making experimental charges containing Co in the range 0.01–0.10 *apfu*.

#### Monosulfide solid-solution $(Fe,Co,Ni)_{1-x}S$

Monosulfide solid-solution is present in all Fe-containing samples, occurring in phase assemblages with  $As_{1-x}S_x$  melt and any of the sulfarsenides or disulfides. It has compositions in the ranges 52.5–54.4 at.% S, 0.0–0.2 at.% As, 6.6–45.4 at.% Fe, 0.1–40.1 at.% Ni, and the sum of metals (*Me*) varies from 45.5 to 47.4 at.%. The average intra-sample variation in *Me* is suspiciously high ( $1\sigma = 0.59$  at.%) and is not matched by a similar variation in S content ( $1\sigma = 0.22$  at.%). The large variations in *Me* contents may well be produced by interference from neighboring grains during EMPA. The  $d(102)$  value is a representative measure of the unit-cell parameter of the *mss* subcell (Morimoto *et al.* 1975), and it varies from 1.974 Å in the member poorest in Fe to 2.064 Å for the pure Fe-member. Values in the lower part of the range (< 2.019 Å) are somewhat uncertain owing to overlap with the (211) reflection of

gersdorffite. In some cases, several peaks were observed in the relevant region; these could either reflect a splitting of  $d(102)$  due to transformation to a lower symmetry during the quench (Tokonami *et al.* 1972, Morimoto *et al.* 1975) or the presence of several *mss* compositions in the sample.

The composition of *mss* from various assemblages is shown in Figures 4 to 9. The tielines between cobaltite and *mss*, from the *Cbt + mss + AsS* assemblage, show a seemingly haphazard orientation in ternary space (Fig. 10), but if one combines them with the S-content of the coexisting phases, a pattern emerges. Figure 11 shows a linear relation between the sulfur content and the relative amount of Ni in cobaltite (the latter calculated as:  $\text{apfu Ni in Cbt} / (\text{apfu Ni in mss} + \text{apfu Ni in Cbt})$ ). At low S contents, Ni is strongly concentrated in cobaltite (85% of Ni), whereas at high S contents, it concentrates in *mss* (68% of Ni). This proves that the

arsenic and sulfur fugacities have a strong influence on the cation distribution of the coexisting phases.

#### Vaesite, $\text{NiS}_2$

Vaesite occurs in equilibrium with combinations of gersdorffite, *mss* and  $\text{As}_{1-x}\text{S}_x$  melt. A limited extent of the Fe- and S-rich side of the vaesite solid-solution volume was determined in these experiments, and the compositions (61.7–64.9 at.% S, 2.2–5.2 at.% As, Fe < 1.4 at.%, Co < 2.3 at.%, 29.4–33.1 at.% Ni) are relatively close to pure vaesite. Vaesite rich in Fe and Co also contains more arsenic, but as there are only three vaesite-bearing samples, this tendency is uncertain. The maximum solubility of Co and Fe in vaesite was not determined in these experiments, and it is very likely that a more extensive or complete solubility exists, as reported by Klemm (1965) and Wyzomirski (1980).

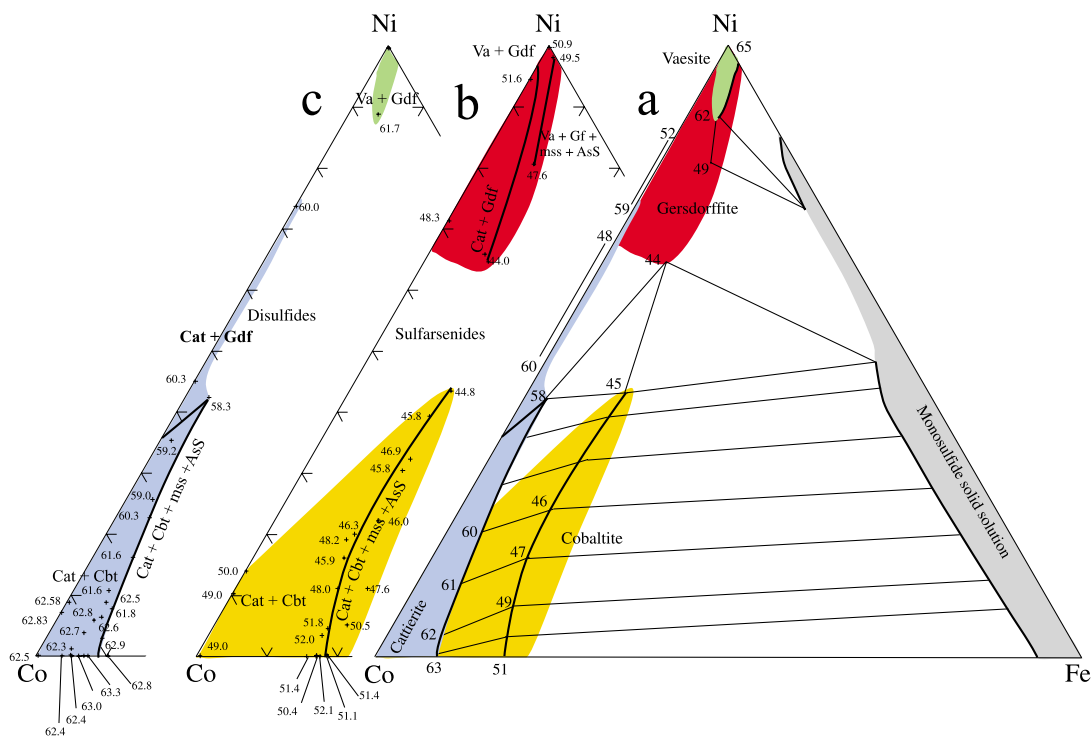


FIG. 12. Phase relations of assemblages of disulfides in equilibrium with sulfarsenides at 650°C. Phases *mss* and  $\text{As}_{1-x}\text{S}_x$  melt also are present in Fe-rich assemblages. The S contents (at.%) are indicated at the data points. These data were presented in detail in Figures 6 and 8. (a) Idealized phase-relations involving disulfides and sulfarsenides. The disulfides are shown superimposed on the sulfarsenides with which they coexist, as if viewing the prism in Figure 14b from the S end. (b) Compositions of the sulfarsenides from (a), with the appropriate phase-assemblage given for each field and along the limits the fields. (c) Compositions of the relevant disulfides with phase assemblages marked. The inset figure in Figure 13 shows the location of Figure 12 in the *Me* – *As* – *S* triangle. The phases are catterrite (blue), vaesite (green), cobaltite (yellow), gersdorffite (red) and *mss* (grey).

### Summary of phase relations at 650°C

The most convenient presentation of these phase relations is the (Fe-Co-Ni)(As,S)<sub>2</sub> prism, *i.e.*, a prism with the base equal to the Fe-Co-Ni triangle and a virtual vertical axis equal to S. This gives a sufficiently correct rendering for  $Me(S,As)_2$  phases, because at.% As approximates [66.67 - at.% S]. The monosulfide solid-solution has metal and S contents that place it outside the  $Me(As,S)_2$  prism, but it incorporates insignificant amounts of As. Therefore, *mss* compositions were presented in the (Fe-Co-Ni)-S diagram as well. The  $As_{1-x}S_x$  melt cannot be shown in this manner, but the log  $a(S_2)$  derived from the composition of the melt has been written along the relevant tielines.

The As-rich surface of the disulfide solid-solution and the S-rich compositions of the coexisting sulfarsenides

were constructed from the data presented in Figures 6 to 10 (Fig. 12). The average compositions from each sample are shown as data points, and the average sulfur content (atomic % of total) is listed adjacent to the data points. The phase associations are listed in the compositional fields, and the solid lines mark the univariant phase-assemblages limiting or separating fields. The left-hand part of Figure 12 shows the compositions of the disulfides, the central part shows the composition of the sulfarsenides, and the right-hand part shows an idealized presentation of phase relations involving disulfides coexisting with sulfarsenides.

The continuation of the cobaltite and gersdorffite solid-solutions toward S-poor compositions, as well as of the coexisting *mss*, are idealized in Figure 13. The Cbt + *mss* + AsS field of the cobaltite solid-solution stretches toward compositions richer in Fe and As. The

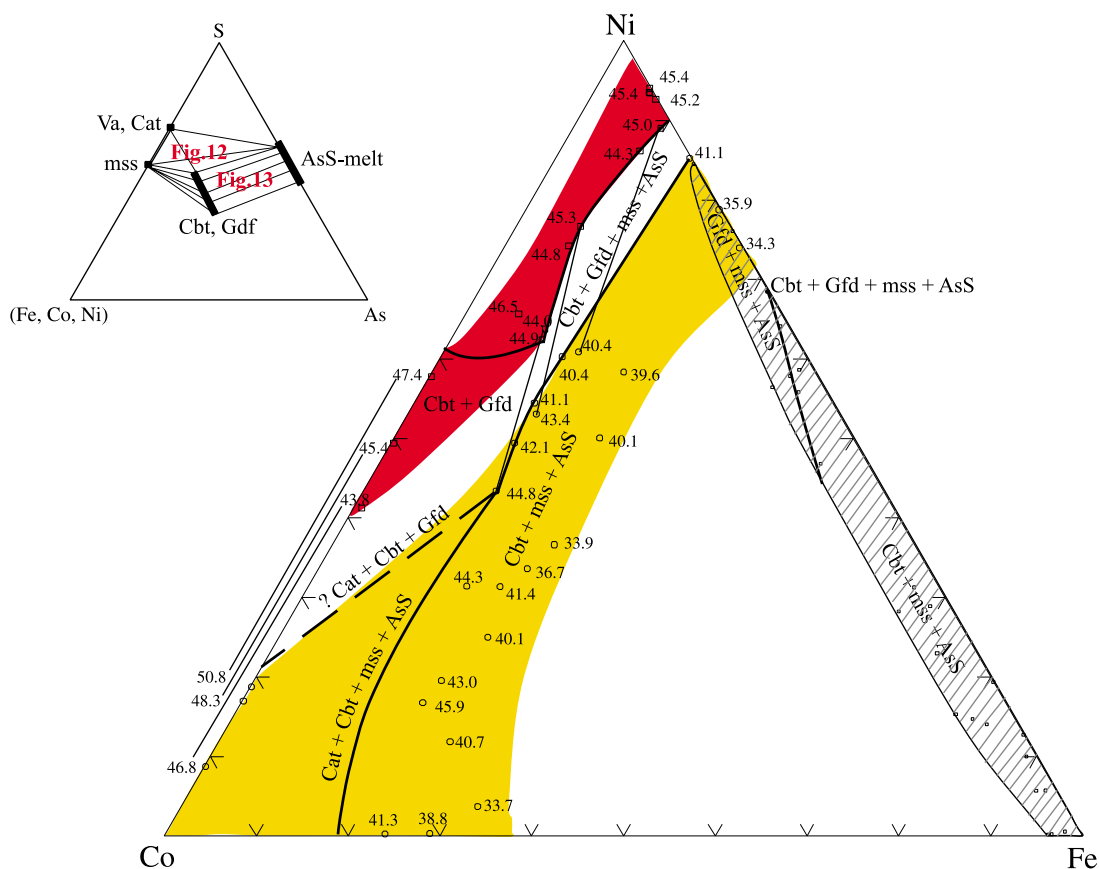


FIG. 13. Summary of the phase relations involving cobaltite, gersdorffite, *mss* and  $As_{1-x}S_x$  melt at 650°C. This corresponds to assemblages richer in As and Fe than those shown in Figure 12. The S contents (at.%) are given alongside the data points, and the phase assemblage is listed alongside the appropriate fields and lines. The inset figure shows the location of Figures 12 and 13 in the  $Me-As-S$  triangle. The phases are cobaltite (yellow), gersdorffite (red) and *mss* (hatched). These data were shown in detail in Figures 7 and 10.

Fe-, As-rich limits of this solid solution were not determined in these experiments. Toward S-rich compositions, the Cbt + *mss* + AsS field of the cobaltite solid-solution is limited by equilibria with cattierite or gersdorffite. Cobaltite from the Gdf + Cbt + *mss* + AsS assemblage is slightly poorer in sulfur than the coexisting gersdorffite (Fig. 13), but the inverse relation is seen in the Cbt + Gdf assemblage found along the Co–Ni join (Fig. 9c). Hence, the Cbt + Gdf assemblage describes the S- and Fe-poor side of the cobaltite solid-solution, whereas the Cbt + *mss* + AsS assemblage coexists with the Fe-containing S-rich side. The projection of the *mss* field shown in Figure 13 overlaps the cobaltite field, but *mss* contains more sulfur and metals than the sulfarsenides, and does not overlap in compositional space, as illustrated by the inset figure. Figure 14a shows the location of all the observed solid-solutions in the  $MeX_2$  prism, thereby connecting Figures 12 and 13.

#### THE 500°C EXPERIMENTS

The phase relations in the central portions of the 500°C diagrams are dominated by three five-phase assemblages, Apy + Cbt + Gdf + Py + *mss*, Cbt + Gdf + Py + Cat + *mss* and Gdf + Py + Cat + Va + *mss*, which are schematically presented in Figure 14b. All other phase assemblages are derived from these. The compositions of the five-phase assemblages are given in Table 2.

As was the case with the 650°C experiments, the phase relations determined at 500°C can be viewed as combinations of the phase relations found at each of the corners. In addition to the drastically reduced extent of solid solutions, the main differences are found in the Fe corner, where Apy + Py + *mss* are stable instead of *mss* + AsS. According to Clark (1960), this phase assemblage is not stable above 491°C, being replaced by the Apy + *mss* + AsS assemblage in the temperature interval 491–688°C. No instances of  $As_{1-x}S_x$  melt were found during the 500°C experiments, whereas pyrite was found in all Fe-containing samples.

#### Arsenopyrite, $FeAsS$

Arsenopyrite coexists with combinations of pyrite, cobaltite, gersdorffite and *mss*. Its composition varies within the limits 33.2–34.3 at.% S, 32.1–33.2 at.% As, 26.5–33.4 at.% Fe, 0.0–5.7 at.% Co and 0.0–1.4 at.% Ni (Fig. 15). Its composition is quite constant with regard to all elements except Co, and there is no connection between the As/S value and cation distribution. The unit cell of arsenopyrite could not be calculated because the peaks heavily overlap with those of pyrite, *mss* and, in some cases, groups of them coalesce into a broad single peak. This left only one to four peaks that can be unambiguously identified, too few to refine a monoclinic unit-cell.

#### Cattierite, $CoS_2$

Cattierite is found coexisting with up to four phases from among cobaltite, gersdorffite, pyrite, vaesite, *mss*, linnaeite and siegenite (Table 1). It contains 1.0–8.5 at.% As, <1.75 at.% Fe and <6.9 at.% Ni (Fig. 16). Ni- and Fe-rich specimens are also rich in As. The cattierite richest in Co is found in the Cbt + Cat + Lin + *mss* assemblage. At the Fe-rich boundary, the cattierite solid-solution coexists with Py. The cattierite richest in Ni coexists with Va, whereas that of intermediate Ni content coexists with Gdf. The unit-cell parameter *a* varies from 5.523(3) Å in Ni-free Fe-bearing cattierite to 5.567(1) Å in Fe-free Ni-bearing cattierite.

#### Cobaltite, $CoAsS$

Cobaltite coexists with up to four of the following phases: arsenopyrite, gersdorffite, cattierite, pyrite, vaesite, *mss* and linnaeite (Table 1). In addition to Co and S, it contains 26.2–34.1 at.% As, 0.1–4.0 at.% Fe and <7.9 at.% Ni (Fig. 15). Co-rich cobaltite coexists with cattierite, Ni-rich compositions occur with vaesite, and the Fe-rich compositions, with pyrite and arsenopyrite. Cobaltite coexists with linnaeite only in assemblages that contain cattierite. Cobaltite rich in Fe has a tendency to contain less sulfur than cobaltite rich in Co and especially Ni. The unit-cell parameter *a* of cobaltite varies from 5.561(4) to 5.580(6) Å, corresponding to Ni-free and Ni-enriched compositions, respectively.

#### Gersdorffite, $NiAsS$

Gersdorffite coexists with all other  $Me(S,As)_2$  phases, as well as with linnaeite and siegenite (Table 1). Gersdorffite rich in Ni and S coexists with vaesite, whereas the Co- and Fe-rich compositions are found in assemblages that contain cobaltite and cattierite or arsenopyrite and pyrite. The composition varies from 35.8–41.3 at.% S, 25.5–30.4 at.% As, <6.4 at.% Fe, <5.4 at.% Co and 27.2–32.6 at.% Ni (Fig. 15). Samples rich in Ni are also rich in S, whereas samples rich in Fe are poor in S. The unit-cell parameter *a* of gersdorffite from vaesite-free assemblages varies from 5.616(3) to 5.689(8) Å, where high contents of Fe yield a small unit-cell parameter and *vice versa*. The true unit-cell parameter of Ni-rich gersdorffite was not found, and the unit cells determined for these are most likely too small owing to X-ray-diffraction interference from coexisting vaesite.

#### Pyrite, $FeS_2$

Pyrite is the dominant mineral in these experiments, and it is found in all Fe-containing samples. Fe-rich pyrite coexists with any four phases, including all the sulfarsenides, whereas in assemblages richer in Ni and

Co, it coexists with cattierite or vaesite (Table 1, Fig. 16). The exact compositional boundaries between pyrite from different phase-associations with the sulfarsenides are uncertain, as the data are ambiguous. This unclear picture is reflected by the PXRD data (presented in Fig. 4), where there is no clear correlation between the unit-cell parameter  $a$  and the average ionic radius or sulfur content. This can only be explained by arguing that the composition of pyrite varies significantly within each sample, suggesting that it is less well equilibrated than the other phases. The composition of pyrite varies within the ranges (62.0–66.4 at.% S, 0.1–4.5 at.% As, 25.1–32.5 at.% Fe, 25.1–8.5 at.% Co and <5.4 at.% Ni), and the unit-cell parameter  $a$  varies from 5.411(3) to 5.439(2) Å.

#### *Vaesite, NiS<sub>2</sub>*

Vaesite is found in equilibrium with gersdorffite, cattierite and pyrite (Fig. 16). Its composition is limited to the range 64.2–66.2 at.% S, 0.8–2.4 at.% As, <1.1 at.% Fe, 0–2.6 at.% Co and 30.4–32.0 at.% Ni. Ni-rich vaesite coexists with gersdorffite, Co-rich vaesite, with cattierite and linnaeite or siegenite, and Fe-rich vaesite, with pyrite and *mss*. The variation in S content is small compared to the standard deviation within each sample, and shows no correlation with phase assemblage or cation distribution. The observed variation in sulfur content is thus chiefly due to interference from gersdorffite during EMPA. The unit-cell parameter  $a$  varies from 5.622(2) to 5.643(2) Å, and was found to vary independently of chemical composition. The random variation is probably caused by different degrees of peak overlap between Va and Gdf. Vaesite compositions show a narrow variation, so that most of the variation in unit-cell  $a$  must be attributed to overlap with gersdorffite peaks.

#### *Mss (Fe,Ni)<sub>1-x</sub>S, linnaeite Co<sub>3</sub>S<sub>4</sub> and siegenite Ni<sub>3</sub>S<sub>4</sub>*

The compositions of the metal-rich phases *mss* (53.0–54.9 at.% S, 0.1–0.7 at.% As, 20.7–45.5 at.% Fe, <3.7 at.% Co and <24.3 at.% Ni), linnaeite (56.9–58.3 at.% S, 0.1–0.8 at.% As, <1.0 at.% Fe, 40.1–41.3 at.% Co and <1.9 at.% Ni) and siegenite (57.5 at.% S, 0.11 at.% As, 0.3 at.% Fe, 24.9 at.% Co and 17.2 at.% Ni) do not show a systematic compositional variation similar to that exhibited by the other phases present (Fig. 17). Linnaeite and siegenite are only present in limited amounts, and it is uncertain whether these thiospinels represent equilibrium compositions. The As content of these phases shows a very large variation compared to the standard deviation, and we therefore believe it to be heavily influenced by interference from neighboring grains. The true As content is most likely <0.1 at.%.

*Mss* is common in most samples, and its composition is remarkably constant. The compositions are concentrated at the low-Ni end of the solid-solution field,

and they are relatively sulfur-rich (see above). An exception from this is *mss* from assemblages containing vaesite or linnaeite, which is *mss* substantially richer in Ni or Co. The  $d(102)$  values of both groups lie below the lower limit of the corresponding  $d$ -mean of Morimoto *et al.* (1975), which varies from 2.064 to 2.072 Å for *mss* containing 52.15–52.8 at.% S. Only a single sharp reflection is seen, identifying it as one of the types of hexagonal *mss* (Tokonami *et al.* 1972, Morimoto *et al.* 1975). For the Fe-rich *mss*,  $d(102)$  varies from 2.041 to 2.053 Å, whereas it varies from 2.024 to 2.028 Å for the Ni-rich *mss* coexisting with vaesite. Inserting the content of iron of the *mss* richest in Fe (54.18 at.%, 0.14 at.% As, 45.48 at.% Fe, 0.13 at.% Co and 0.08 at.% Ni) into the equation (2) of Morimoto *et al.* (1975) gives a  $d$ -mean of 2.0466 Å, which is almost equal to the measured 2.0472 Å. For this purpose, the minor amounts of Co, Ni and As were added to Fe (*i.e.*, Fe = 100 – at.% S). We thereby assume that Fe, Co, Ni and As all would contribute to an increase in unit-cell size.

Several authors have reported a much larger solubility of Co and Ni in *mss* at comparable or lower temperatures. According to Craig *et al.* (1968), *mss* coexisting with Py at 400°C should contain up to approximately 70% Ni of the total Fe + Ni. *Mss* coexisting with linnaeite and cattierite at 500°C should contain 75% Co of the sum Fe + Co (Wyszomirski 1980). The introduction of As into the system is a possible explanation of this discrepancy. The sulfarsenides and the As-bearing disulfides apparently show a considerable affinity for Co and Ni, and thereby deplete the *mss* of these elements. This explanation is in agreement with the positive influence of sulfur content on the concentration of Co and Ni in *mss* relative to cobaltite (Fig. 11).

#### *Summary of phase relations at 500°C*

The phase relations shown in Figures 15 and 16 are sections through the  $Me(S,As)_2$  prism illustrated in Figure 14, which also shows the Apy + Cbt + Gdf + Py + *mss*, Cbt + Gdf + Py + Cat + *mss* and Gdf + Py + Cat + Va + *mss* assemblages. The fields of the sulfur-rich surfaces of the respective sulfarsenide solid-solutions are shown in Figure 15. The coexisting  $Me(S,As)_2$  phase is indicated in the relevant fields, and the phase assemblage is shown by symbols. In the cobaltite field, there is ambiguity concerning the exact location of the boundaries separating Apy, Gdf and Py. The relevant boundaries are therefore stippled.

The disulfides coexisting with the sulfarsenides shown in Figure 15 are illustrated in Figure 16. The fields shown here represent the As-rich sides of the disulfide solid-solutions. Cattierite and vaesite both show limited solubility of Fe, whereas pyrite can contain significant amounts of both Co and Ni. Exact bound-

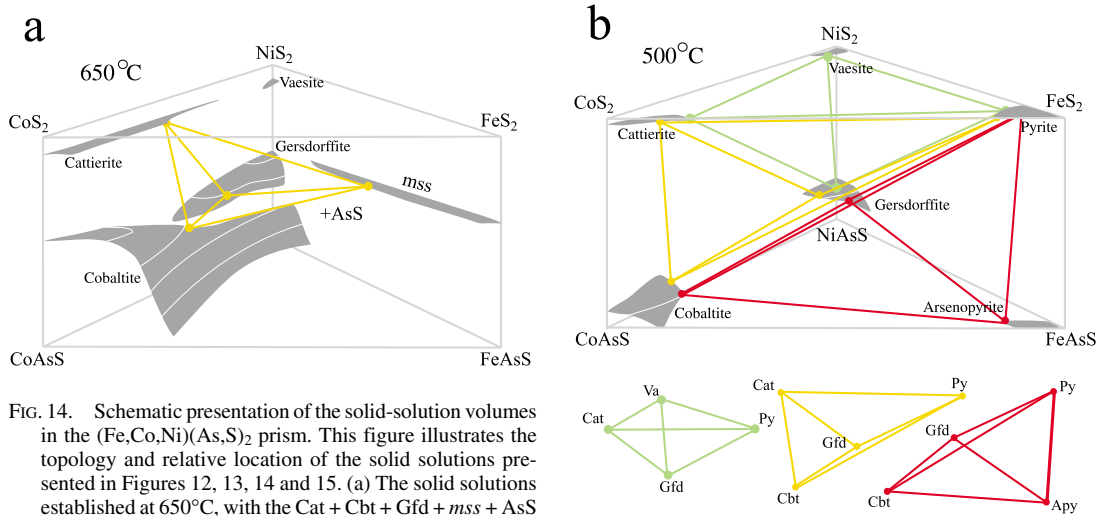


FIG. 14. Schematic presentation of the solid-solution volumes in the  $(\text{Fe,Co,Ni})(\text{As,S})_2$  prism. This figure illustrates the topology and relative location of the solid solutions presented in Figures 12, 13, 14 and 15. (a) The solid solutions established at  $650^\circ\text{C}$ , with the  $\text{Cat} + \text{Cbt} + \text{Gfd} + \text{mss} + \text{AsS}$  assemblage marked. The *mss* solid solution is projected into the prism; we plot its sulfur content at the corresponding level of the prism, i.e.,  $x$  in  $\text{MeAs}_{2-x}\text{S}_x$  is equal to at.% S/33.33. (b) The solid solutions found at  $500^\circ\text{C}$  with the dominant assemblages shown both in the  $(\text{Fe,Co,Ni})(\text{As,S})_2$  prism and below. The sulfarsenides are shown in detail in Figure 15, and the disulfides, in Figure 16. The assemblages are  $\text{Cbt} + \text{Gfd} + \text{Py} + \text{Cat}$  (yellow),  $\text{Gfd} + \text{Py} + \text{Cat} + \text{Va}$  (green) and  $\text{Apy} + \text{Cbt} + \text{Gfd} + \text{Py}$  (red).

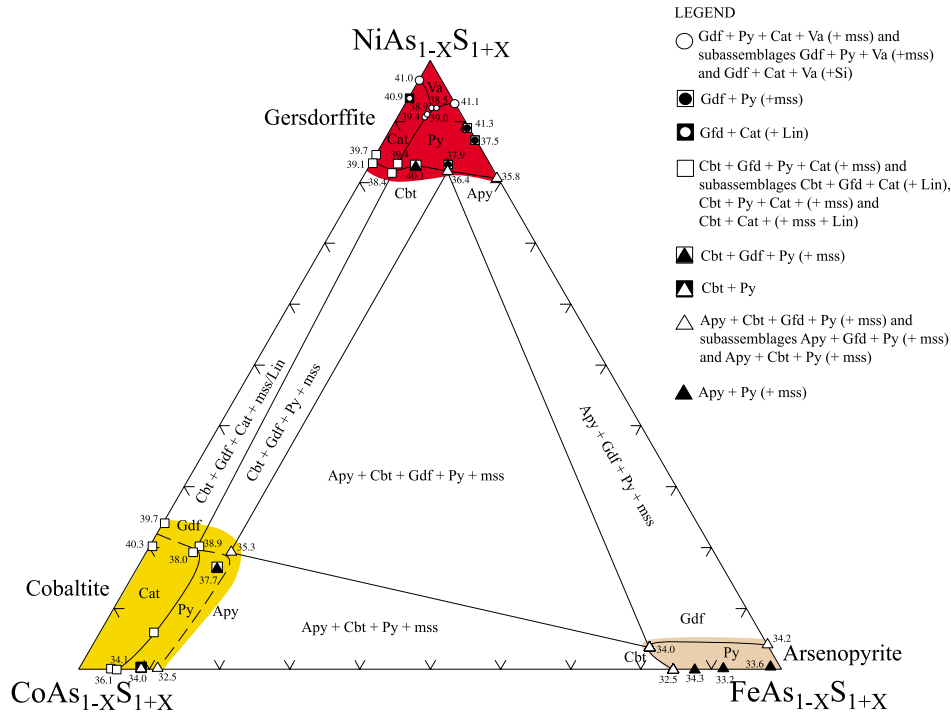


FIG. 15. Compositions and phase assemblages of sulfarsenides at  $500^\circ\text{C}$ . The solid-solution fields correspond to the S-rich side of the respective solid-solutions, located close to the base of the prism in Figure 14b. These sulfarsenides coexist with disulfides, shown in Figure 16. The phase assemblage of each sample is shown alongside the legend, and its interpretation in terms of phase boundaries is drawn in the different solid-solution fields. The phase stated to be present in each field indicates which phase the given solid-solution member coexists with. Uncertain boundaries are stippled. The S content (at.%) is indicated at each data point.

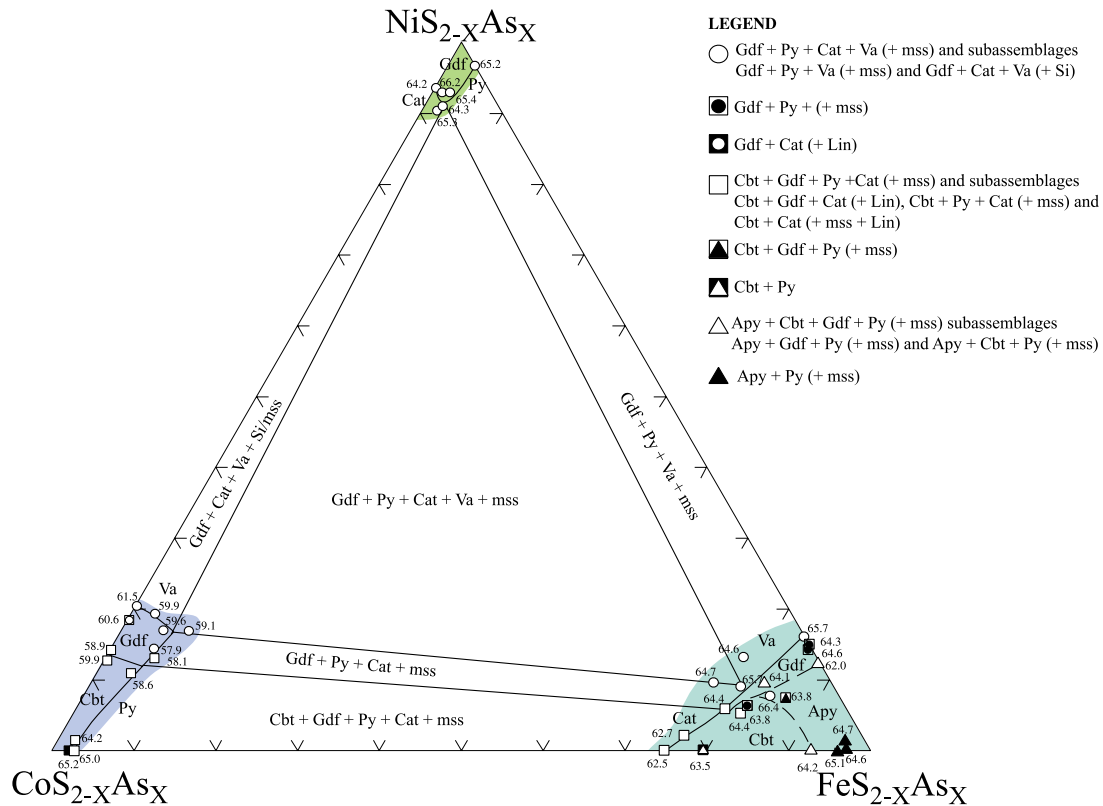


FIG. 16. Disulfide compositions and phase assemblages at 500°C. These solid-solution fields correspond to the As-rich sides of the disulfide solid-solutions and coexist with the sulfarsenides in Figure 15. They are located close to top of the prism in Figure 14b. The phase assemblage of each sample is shown alongside the legend, and its interpretation in terms of phase boundaries is drawn on the different solid-solution fields. The phase stated to be present in each field indicates which phase the given solid-solution member coexists with. The S contents (at.%) are written alongside each data point.

aries of the different phase-assemblages within the pyrite solid-solution are somewhat uncertain, as the data produce an ambiguous picture. The cation contents of the metal-rich phases, *mss*, siegenite and linnaeite, are shown in Figure 17. These phases do not describe continuous solid-solutions, and it is questionable whether all the compositions obtained here represent equilibrium assemblages.

#### DISCUSSION

A comparison between the EMPA and the PXRD data reveals serious analytical problems with regard to the interpretation of the PXRD data. The compositional and dimensional similarity of coexisting homeotypic phases led to the refinement of unit-cell parameters that are the weighted average of the phases present. The PXRD data from the 650°C experiments suggest the presence of only one to two cubic phases, where up to

three were encountered. This problem underscores the need for careful examination of experimental textures, a sufficient amount of EMPA measurements, as well as critical evaluation of overlaps in the PXRD data. Furthermore, the validity of the observed phase-relations can be checked by comparing them with related experimental works as well as natural assemblages.

A literature review shows that only a few of the phase assemblages presented here can be directly compared with similar phase-assemblages from experimental work on related systems. Several authors have reported a complete solid-solution between the Co and Ni members of both the sulfarsenide and the disulfide solid-solutions, as well as an extensive solid-solution toward the Fe end-members (Klemm 1965, Steger *et al.* 1974, Wyszomirski 1980). Such a solubility of iron is not exhibited by any of the corresponding phases found in this study. The most important difference is the separation of the cobaltite-gersdorffite solid-solution series

into two phases at 650°C, where Klemm (1965) reported a complete solid-solution. The disagreement may be real and can be explained by the different As/S values of the two datasets. This explanation is supported by investigations of an As-rich section, in which an almost complete solid-solution between gersdorffite and cobaltite was found (Hem & Makovicky 2004).

The assemblages found in each of the corners generally correspond well with those reported in the literature (Yund 1962, Barton 1969, Bayliss 1969, Maurel & Picot 1974). Sulfur-rich (52 at.%) cobaltite coexisting with catterite at 550°C was reported by Bayliss (1969), and a complete solid-solution (at 800°C) between CoAsS and CoAs<sub>0.5</sub>S<sub>1.5</sub> was reported by Maurel & Picot (1974). These S-contents are lower than those found in the present study at 500°C, but similar to those found at 650°C. Gersdorffite coexisting with vaesite at 700°C was reported to contain substantially less S (37 at.%; Yund 1962) than found in this study. Some of these differences can be attributed to the analytical methods used, as the quoted compositions were found on the basis of the charge composition in conjunction with PXRD, and not from EMPA data. Peak overlap between the patterns of different  $MX_2$  phases must have caused significant problems, which also would apply to the work of Klemm (1965).

Another difference between our findings and results in the literature is the Apy + Py + *mss* assemblage de-

termined in the 500°C experiments. Clark (1960) reported the Apy + Py + *mss* assemblage to be stable only at temperatures below 491°C. This relatively small discrepancy can be explained by the potential effect of Co and Ni on the thermal stability of pyrite, as no Co–Ni-free experiments were made. One must also keep in mind the uncertainty in temperature measurements, which are  $\pm 2.8^\circ\text{C}$  for this study and  $\pm 12^\circ\text{C}$  for Clark (1960). On this basis, it seems likely that stability maximum of the Apy + Py + *mss* assemblage is located slightly above 500°C.

The solubility of Co (at 500° and 650°C) and Ni (at 500°C) in *mss*, and the solubility of Ni in linnaeite (at 500°C) are drastically smaller than reported for assemblages in the ternary system (Wyszomirski 1980). Overall, Co and Ni tend to be concentrated in the As-containing phases (Fig. 11).

Some of the observed phase-assemblages do not have natural counterparts. The paragenesis richest in S in which gersdorffite and cobaltite occur is associated with pyrite (Burke & Zakrzewski 1983, Kerestejian 1984, Laroussi *et al.* 1992, Marcoux *et al.* 1996, Klemm & Krätner 2000, among others), whereas in this study they are found coexisting also with catterite and vaesite. In nature, catterite and vaesite most commonly occur in association with the thiospinels of Co, Ni and Cu, as well as with pyrite (Hudson & Groves 1974, Ostwald 1980, Strashimirov *et al.* 2002). Natural assemblages

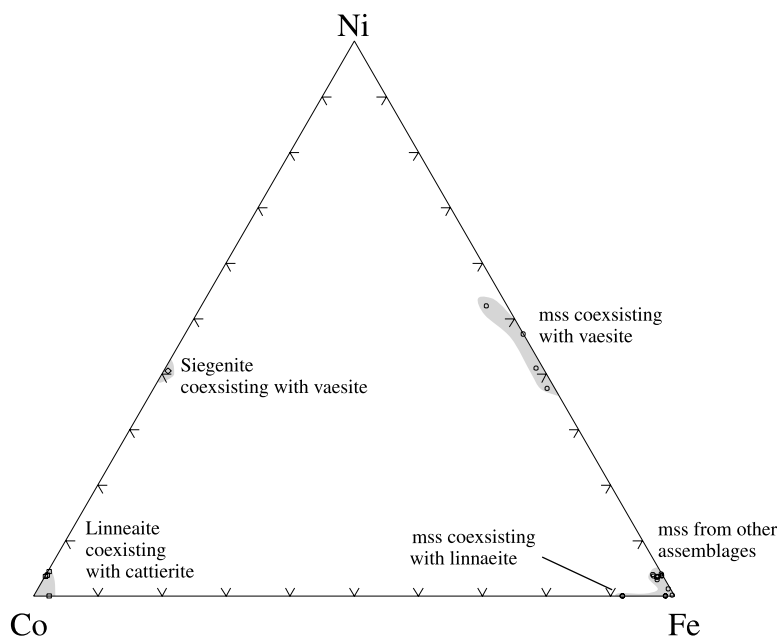


FIG. 17. Compositions of the metal-rich phases *mss*, linnaeite and siegenite. *Mss* compositions define several groups; those coexisting with vaesite, one coexisting with linnaeite, and those coexisting with *mss* from any other assemblages.

from comparable temperatures (500–650°C) involving cattierite and vaesite have not been reported, and even at low temperatures, there are no records of sulfarsenides forming in equilibrium with either vaesite or cattierite. There are three explanations for this: 1) It is a geochemical feature, as no alternative phase-assemblage has been reported for the bulk composition in question. 2) The analogous natural assemblages may have re-equilibrated. 3) The differences may be caused by the presence of other elements in the natural system. This addition may stabilize phases that concentrate elements involved in the sulfide phase-equilibria.

#### CONCLUSIONS

The phase relations in the  $MeS_2$ – $MeAsS$  system ( $Me = Fe, Co, Ni$ ) are dominated at 650°C by phase assemblages involving cobaltite, gersdorffite, cattierite or vaesite coexisting with monosulfide solid-solution +  $As_{1-x}S_x$  melt in Fe-bearing assemblages. Vaesite was not found coexisting with cattierite or cobaltite. The sulfarsenides are richer in sulfur than their natural analogues, but comparable with reports from earlier works. The observed phase-relations show the drastic effect of the ratio As/S on the solid-solution fields of the Co–Ni sulfarsenides.

At 500°C, the five-phase assemblages  $Apy + Cbt + Gdf + Py + mss$ ,  $Cbt + Gdf + Py + Cat + mss$  and  $Gdf + Py + Cat + Va + mss$  dominate the compositional space. All phases show reduced extents of solid solution, and the compositions are generally closer to stoichiometry. Siegenite and linnaeite was also found in Ni- and Co-rich samples.

There are no natural analogues to the vaesite- or cattierite-bearing assemblages observed, as these phases in nature usually form at significantly lower temperatures. As the observed relations show a reasonable agreement with published investigations of related subsystems, the lack of natural counterparts is most likely caused by the increased complexity of the natural systems.

#### ACKNOWLEDGEMENTS

This study is part of a Ph.D. study by S.H. financed by the Faculty of Science at the University of Copenhagen. The electron-microprobe analyses and the X-ray powder diffraction were funded by the Danish Natural Research Council. The assistance and advice of Berit Wenzell, Helene Almind, John Rose Hansen, Milota Makovicky, Phillipe Leone and, last but not least, Yves Moëlo, are gratefully acknowledged. The thoughtful comments of Paul Barton, Robert F. Martin and Robert R. Seal II were greatly appreciated.

#### REFERENCES

- BARNES, S.J. & HILL, R.E.T. (2000): Metamorphism of komatiite-hosted nickel sulfide deposits. *In* *Metamorphosed and Metamorphogenic Ore Deposits. Rev. Econ. Geol.* **11**, 203-215.
- BARTON, P.B. (1969): Thermochemical study of the system Fe–As–S. *Geochim. Cosmochim. Acta* **33**, 841-857.
- BAYLISS, P. (1968): The crystal structure of disordered gersdorffite. *Am. Mineral.* **53**, 290-293.
- \_\_\_\_\_ (1969): Isomorphous substitution in synthetic cobaltite and ullmannite. *Am. Mineral.* **54**, 426-430.
- \_\_\_\_\_ & STEPHENSON, N.C. (1967): The crystal structure of gersdorffite. *Mineral. Mag.* **36**, 38-42.
- BURKE, E.A.J. & ZAKRZEWSKI, M.A. (1983): A cobalt-bearing sulfide–arsenide assemblage from the Nord mine (Finsshytteberg), Sweden: a new occurrence of clinosafflorite. *Can. Mineral.* **21**, 129-136.
- CLARK, L.A. (1960): The Fe–As–S system: phase relations and applications. *Econ. Geol.* **55**, 1345-1381.
- CRAIG, J.R., NALDRETT, A.J. & KULLERUD, G. (1968): The Fe–Ni–S system. 3. 400°C isothermal diagram. *Carnegie Inst. Wash., Yearbook* **66**, 440-441.
- \_\_\_\_\_ & SCOTT, S.D. (1974): Sulfide phase equilibria. *In* *Sulfide Mineralogy* (P.H. Ribbe, ed.). *Rev. Mineral.* **1**, CS51-CS110.
- ELLIOT, N. (1960): Interatomic distances in  $FeS_2$ ,  $CoS_2$  and  $NiS_2$ . *J. Phys. Chem. Solids* **33**, 903-905.
- EN NACRI, A. (1995): *Contribution à l'étude du district à Co, As, (Ni, Au, Ag) de Bou Azzer, Anti-Atlas (Maroc). Données minéralogiques et géochimiques; étude des inclusions fluides.* Thèse de doctorat, Univ. d'Orléans, Orléans, France.
- FLEET, M.E. & BURNS, P.C. (1990): Structure and twinning of cobaltite. *Can. Mineral.* **28**, 719-723.
- FURUSETH, S. & KJEKSHUS, A. (1969): On the magnetic properties of  $CoSe_2$ ,  $NiS_2$  and  $NiSe_2$ . *Acta Chem. Scand.* **23**, 2325-2334.
- GIESE, R.F. & KERR, P.F. (1965): The crystal structure of ordered and disordered cobaltite. *Am. Mineral.* **50**, 1002-1014.
- GRORUD, H.-F. (1997): Textural and compositional characteristics of cobalt ores from the Skutterud mines of Modum, Norway. *Norsk Geol. Tidsskr.* **77**, 31-38.
- HANUS, D. & MUSHI, J. (1971): Cattierit–Vaesit–Mischkristalle, eine röntgenographische Bestimmung der Reihe  $CoS_2$  –  $NiS_2$ . *Neues Jahrb. Mineral., Monatsh.*, 379-382.

- HEM, S.R. & MAKOVICKY, E. (2004): The system Fe–Co–Ni–As–S. II. Phase relations in the (Fe,Co,Ni)As<sub>1.5</sub>S<sub>0.5</sub> section at 650° and 500°C. *Can. Mineral.* **42**, 63-86.
- HUDSON, D.R. & GROVES, D.I. (1974): The composition of violarite coexisting with vaesite, pyrite and millerite. *Econ. Geol.* **69**, 1335-1340.
- KERESTEJIAN, T. (1984): Alloclasite–cobaltite paramorphic transformation in the ores of the Vatia deposit, West Balkan Mountain. *Geologica Balcanica* **14**, 73-78.
- KLEMM, D.D. (1965): Synthesen und Analysen in den Dreiecksdiagrammen FeAsS–CoAsS–NiAsS und FeS<sub>2</sub>–CoS<sub>2</sub>–NiS<sub>2</sub>. *Neues Jahrb. Mineral., Abh.* **103**, 205-255.
- \_\_\_\_\_ & KRÄUTNER, H.G. (2000): Hydrothermal alteration and associated mineralization in the Freda–Rebecca gold deposit – Bindura District, Zimbabwe. *Mineral. Deposita* **35**, 90-108.
- KRETSCHMAR, U. & SCOTT, S.D. (1976): Phase relations involving arsenopyrite in the system Fe–As–S and their application. *Can. Mineral.* **14**, 364-386.
- KULLERUD, G., YUND, R.A. & MOH, G.H. (1969): Phase relations in the Cu–Fe–S, Cu–Ni–S and Fe–Ni–S system. In *Magmatic Ore Deposits* (H.D.B. Wilson, ed.). *Econ. Geol., Monogr.* **4**, 323-343.
- LAMPRECHT, G. (1978): Phasengleichgewichte im System Co–Ni–S unterhalb 1000°C. *Neues Jahrb. Mineral., Monatsh.*, 176-191.
- LAROUSI, A., MOËLO, Y. & YAMAN, S. (1992): Study of cobaltite and alloclasite in Esendemir skarn-type ore deposit (Ulukisla-Nidge) by electron microprobe technique. *Turkish J. Earth Sci.* **1**, 57-61.
- MARCOUX, E., MOËLO, Y. & LEISTEL, J.M. (1996): Bismuth and cobalt minerals as indicators of stringer zones to massive sulphide deposits, Iberian Pyrite Belt. *Mineral. Deposita* **31**, 1-26.
- MAUREL, C. & PICOT, P. (1974): Stabilité de l'alloclasite et de la cobaltite dans le système Co–As–S et Co–Ni–As–S. *Bull. Soc. fr. Minéral. Cristallogr.* **97**, 251-256.
- MORIMOTO, N., GYOBU, A., TSUKUMA, K. & KOTO, K. (1975): Superstructures and nonstoichiometry of intermediate pyrrhotite. *Am. Mineral.* **60**, 240-248.
- NOWACKI, E., SCHWARZENBACH, D., GONSCHOREK, W. & HAHN, T. (1989): Deformationsdichten in CoS<sub>2</sub> and NiS<sub>2</sub> mit Pyritstruktur. *Z. Kristallogr.* **186**, 213-215.
- OSTWALD, J. (1980): Notes on a Co–Ni disulphide and a Co–Ni–Fe thiospinel from the Kalgoorlie district, Western Australia. *Mineral. Mag.* **43**, 950-951.
- PETRUK, W., HARRIS, D.C. & STEWART, J.M. (1971): Characteristics of the arsenides, sulpharsenides, and antimonides. *Can. Mineral.* **11**, 150-186.
- PRATT, J.L. & BAYLISS, P. (1979): Crystal-structure refinement of cattierite. *Z. Kristallogr.* **150**, 163-167.
- SATO, T. & SHIMAZAKI, Y. (1975): Vaesite from the Uchinotai deposits, Kosaka mine, Japan. *Mineral. J.* **7**, 431-437.
- SHANNON, R.D. (1976): Revised effective ionic radii and systematic studies of interatomic distances in halides and chalcogenides. *Acta Crystallogr.* **A32**, 751-767.
- STEGER, J.J., NAHIGIAN, H., ARNOTT, R.J. & WOLD, A. (1974): Preparation and characterisation of the solid solution series Co<sub>1-x</sub>Ni<sub>x</sub>AsS (0 ≤ x ≤ 1). *J. Sol. State Chem.* **11**, 53-59.
- STRASHIMIROV, S., PETRUNOV, R. & KANAZIRSKI, M. (2002): Porphyry-copper mineralization in the central Srednogorie zone, Bulgaria. *Mineral. Deposita* **37**, 587-598.
- TOKONAMI, M., NISHIGUCHI, K. & MORIMOTO, N. (1972): Crystal structure of monoclinic pyrrhotite. *Am. Mineral.* **57**, 1066-1080.
- WAGNER, T. & LORENZ, J. (2002): Mineralogy of complex Co–Ni–Bi vein mineralization, Bieber deposit, Spessart, Germany. *Mineral. Mag.* **66**, 385-407.
- WYSZOMIRSKI, P. (1980): The pure dry Fe–Co–S system at 400° to 1000°C. *Neues Jahrb. Mineral. Abh.* **139**, 131-132.
- YUND, R.A. (1962): The system Ni–As–S: phase relations and mineralogical significance. *Am. J. Sci.* **260**, 761-782.

Received July 26, 2003, revised manuscript accepted December 27, 2003.